JACS
JOURNAL OF THE AMERICAN CHEMICAL SOCIETY
Article
pubs.acs.org/JACS

Sitting Phases of Polymerizable Amphiphiles for Controlled Functionalization of Layered Materials

Jae Jin Bang,[†] Kortney K. Rupp,[†] Shane R. Russell,[†] Shi Wah Choong,[†] and Shelley A. Claridge*[,†,‡]

[†]Department of Chemistry and [‡]Weldon School of Biomedical Engineering, Purdue University, West Lafayette, Indiana 47907, United States

Supporting Information

ABSTRACT: Precisely tailoring surface chemistry of layered materials is a growing need for fields ranging from electronics to biology. For many applications, the need for noncovalently adsorbed ligands to simultaneously control interactions with a nonpolar substrate and a polar solvent is a particular challenge. However, biology routinely addresses a similar challenge in the context of the lipid bilayer. While conventional standing phases of phospholipids (such as those found in a bilayer) would not provide spatially ordered interactions with the substrate, here we demonstrate formation of a sitting phase of polymerizable phospholipids, in which the two alkyl chains extend along the surface and the two ionizable functionalities (a phosphate and an amine) sit adjacent to the substrate and project into the solvent, respectively. Interfacial ordering and polymerization are assessed by high-resolution scanning probe measurements. Water contact angle titrations demonstrate interfacial pK_a shifts for the lipid phosphate but not for the amine, supporting localization of the phosphate near the nonpolar graphite surface.

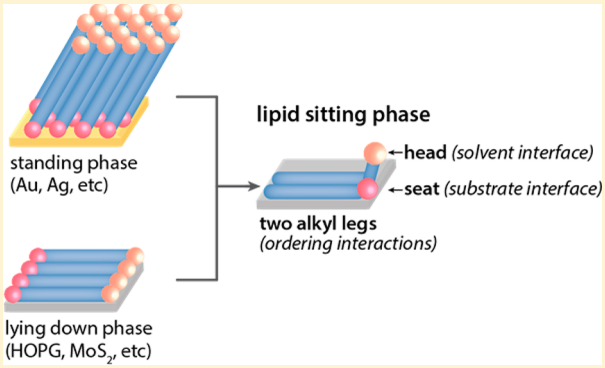

INTRODUCTION

Precisely controlling surface chemistry using self-assembled monolayers (SAMs) and bilayers has been a central focus of research in both synthetic and biological interfaces.[1−4] Much synthetic monolayer chemistry has its basis in the formation of SAMs of alkanethiols on gold and the coinage metals, pioneered by groups including those of Whitesides, Nuzzo, and Allara in the 1980s.[5−8] Standing-up phases of alkanethiol monolayers form based on a combination of covalent or ionic molecule−substrate interactions (e.g., Au−S), strong molecule−molecule van der Waals interactions (e.g., between long alkyl chains) that improve ordering, and a terminal functionality (e.g., $-CH_3$, $-COOH$, $-NH_2$, biotin, DNA) that confers solvent wetting properties and/or selectivity for analytes.[8,9] The surge of interest in colloidal nanocrystals[10−15] has further increased the importance of monolayer chemistry as well as opened entirely new avenues for control of morphology, electronic properties, solubility, and analyte binding.[16−20]

Layered materials (e.g., HOPG, graphene, MoS_2)[21,22] represent a new frontier in utilizing monolayer chemistry to control physical properties and solubility[23,24] but also introduce substantial challenges.[23,25] In single-layer graphene, for instance, *all* atoms are surface atoms and in solution can actually be coordinated through two faces, promising unusually high levels of electronic control through the design and spatial organization of appropriate ligands.[23,24] In contrast with colloidal nanoscopic materials, in which surface curvature typically decreases ligand ordering, the relative flatness of a layered material surface enables ligand ordering that can more strongly resemble SAMs on extended solids.[23,26] However, maintenance of extended π-conjugation in the layer requires noncovalent functionalization, restricting the choice of ligands.[26] These challenges have impacted the utility of graphene and other layered materials in many applications.

Monolayers on highly oriented pyrolytic graphite (HOPG) and graphene are frequently formed on the basis of lying-down phases of molecules;[23,24,26,27] the increased surface area of the molecule−substrate interaction partially offsets the decreased per-atom interaction strength of noncovalent (vs covalent) interactions.[23] Two common classes of adsorption motifs utilized are long alkanes (e.g., 23-carbon tricosane)[28,29] and planar aromatic hydrocarbons (e.g., pyrene, anthracene).[24,30] In noncovalent monolayers, molecule−molecule interactions also play a more prominent role in monolayer stability. These may be based on van der Waals interactions between long alkanes such as tricosane, one or more hydrogen-bonding interactions (e.g., between planar aromatic molecules that display carboxylic acids on their peripheries[31] or β-strand peptides that hydrogen bond to form β-sheets[32,33]), or ionic interactions (e.g., in MOFs[34]).

However, even between very long alkanes, intermolecular forces are relatively weak (~5 kJ/mol of CH_2 between alkane chains[35] and 5−10 kJ/mol of CH_2 for alkane−HOPG

Received: December 16, 2015
Published: March 14, 2016

DOI: 10.1021/jacs.5b13179
J. Am. Chem. Soc. 2016, 138, 4448−4457

interactions[36]). Thus, an extension of this strategy involves noncovalent functionalization using lying-down phases of reactive molecules, followed by polymerization within the layer.[37−39] One such route is based on self-assembly of long-chain carboxylic acids derivatized with an internal diyne that can be photopolymerized to yield a conjugated ene−yne polymer.[37,40−42] A number of studies have examined this reaction on HOPG,[37,43,44] graphene,[45] and MoS_2,[42,46] due to interest in the conductive ene−yne as a molecular wire. Such a strategy can produce monolayers that exhibit some solvent stability,[39,47] but a new challenge arises. Early work on monolayers on bulk metals has demonstrated that functional groups positioned adjacent to a hydrophobic monolayer interface undergo large pK_a shifts (frequently 4 units or more) due to the inability of the interface to stabilize the charged form of the molecule.[48,49] These shifts mean that groups such as carboxylic acids and amines may be predominantly neutral near pH 7 (for instance, in biological buffers), substantially altering their chemical behavior.

Interestingly, a vast amount of biology involving weak acids and bases occurs in a very similar chemical environment: at the periphery of the cellular membrane. Cellular membranes are largely composed of phosphoglycerolipids (typically 60−80%),[50] in which two long hydrophobic acyl chains connect through a three-carbon glycerol backbone to a hydrophilic head. The head is comprised of a phosphate group connected through a short linker to a terminal functional group that is exposed at the solvent interface. The nominal phosphate pK_a values of 1.0 for phosphocholine and 1.7 for phosphoethanolamine[51] mean that the group will remain charged at physiological pH (7.4), even if it undergoes an interfacial pK_a shift. Additionally, the structure of the glycerol backbone facilitates control over headgroup orientation relative to the hydrophobic chains that root it in the bilayer.

Here, we take advantage of the phospholipid architecture to develop an atom-efficient interfacial functionalization strategy that confers the benefits of both standing-up and lying-down monolayers. Lipids in this "sitting-phase" geometry coordinate the surface through two nonpolar alkyl legs, allowing the terminal functional group in the head to project from the interface (Scheme 1). Leveraging noncovalent assembly and subsequent polymerization utilizing polymerizable phospholipids makes fundamental and important differences in the surface chemistry that enable a new level of control over the ligand's substrate and solvent interactions. A critical element of this strategy is the elevation of the terminal functional groups above the substrate and the monolayer to reduce interfacial pK_a shifts. Even modest separation also increases steric accessibility, which has previously been found to facilitate binding of analytes from solution.[52,53]

RESULTS AND DISCUSSION

Self-Assembled Sitting Phases of Diyne Phospholipids. As a starting point for developing a sitting-phase ligand chemistry for layered materials, we first test the ability of polymerizable diyne phospholipids[54,55] to self-assemble into appropriate structural elements. Previous studies of diyne phospholipids in standing-phase monolayers and bilayers indicate that the headgroup tilts; as a result, the two functional alkyl chains penetrate different distances into the bilayer.[56] Thus, when the monolayer is polymerized, the two functional groups join two different polymer chains in the membrane, resulting in low molecular weight cross-linked polymers very different from the high molecular weight linear polymers that would be necessary to stabilize the sitting-phase monolayers targeted here.

Scheme 1. Topochemical Polymerization of Diyne Lipids

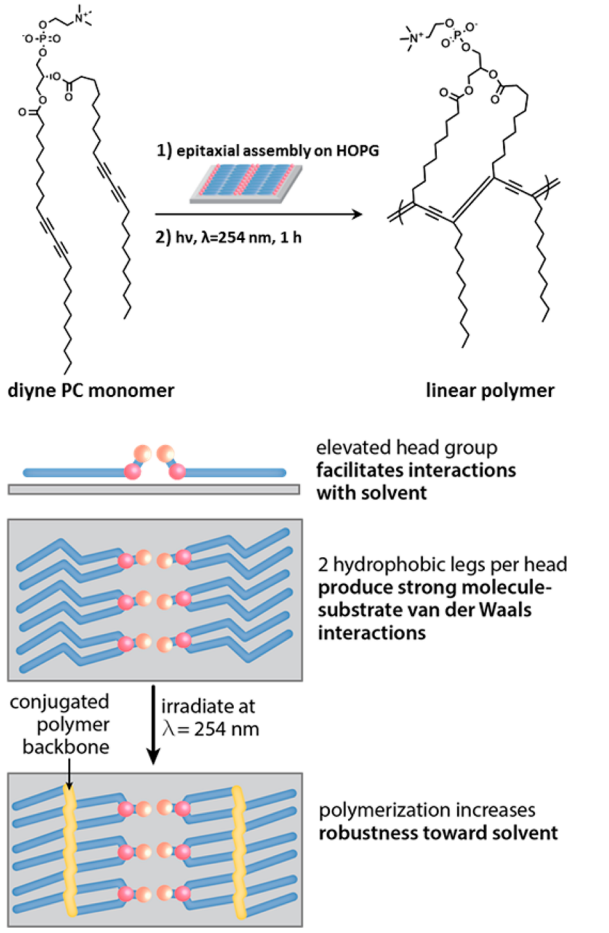

Monolayers of diyne amphiphiles were prepared either by drop-casting a small amount of dilute amphiphile in organic solvent or through Langmuir−Schaefer deposition (see the Experimental Methods for details). Because monolayers of fatty acids such as pentacosadiynoic acid (PCDA) have been prepared previously, we compared self-assembled structures of PCDA (Figure 1a) and two polymerizable phospholipids: 1,2-bis(10,12-tricosadiynoyl)-*sn*-glycero-3-phosphocholine (diyne PC, Figure 1b) and 1,2-bis(10,12-tricosadiynoyl)-*sn*-glycero-3-phosphoethanolamine (diyne PE, Figure 1c). The two phospholipids differ only in the structure of the terminal headgroup functionality; diyne PE terminates in a primary amine, which may be charged or neutral depending on pH and solvent, while the diyne PC terminates in a quaternary ammonium group, which remains charged under all pH and solvent conditions.

A combination of atomic force microscopy (AFM), semi-empirical molecular modeling, and molecular dynamics simulation was used to examine molecular adsorption geometry. First, we assessed structural features in AFM images to address the question of whether molecules assemble head-to-head, creating double rows of headgroups with a ∼6 nm periodicity (Scheme 1), or head-to-tail, resulting in single rows of headgroups with ∼3 nm periodicity. Second, because the molecules can adsorb through two chemically different faces,

DOI: 10.1021/jacs.5b13179
J. Am. Chem. Soc. 2016, 138, 4448−4457

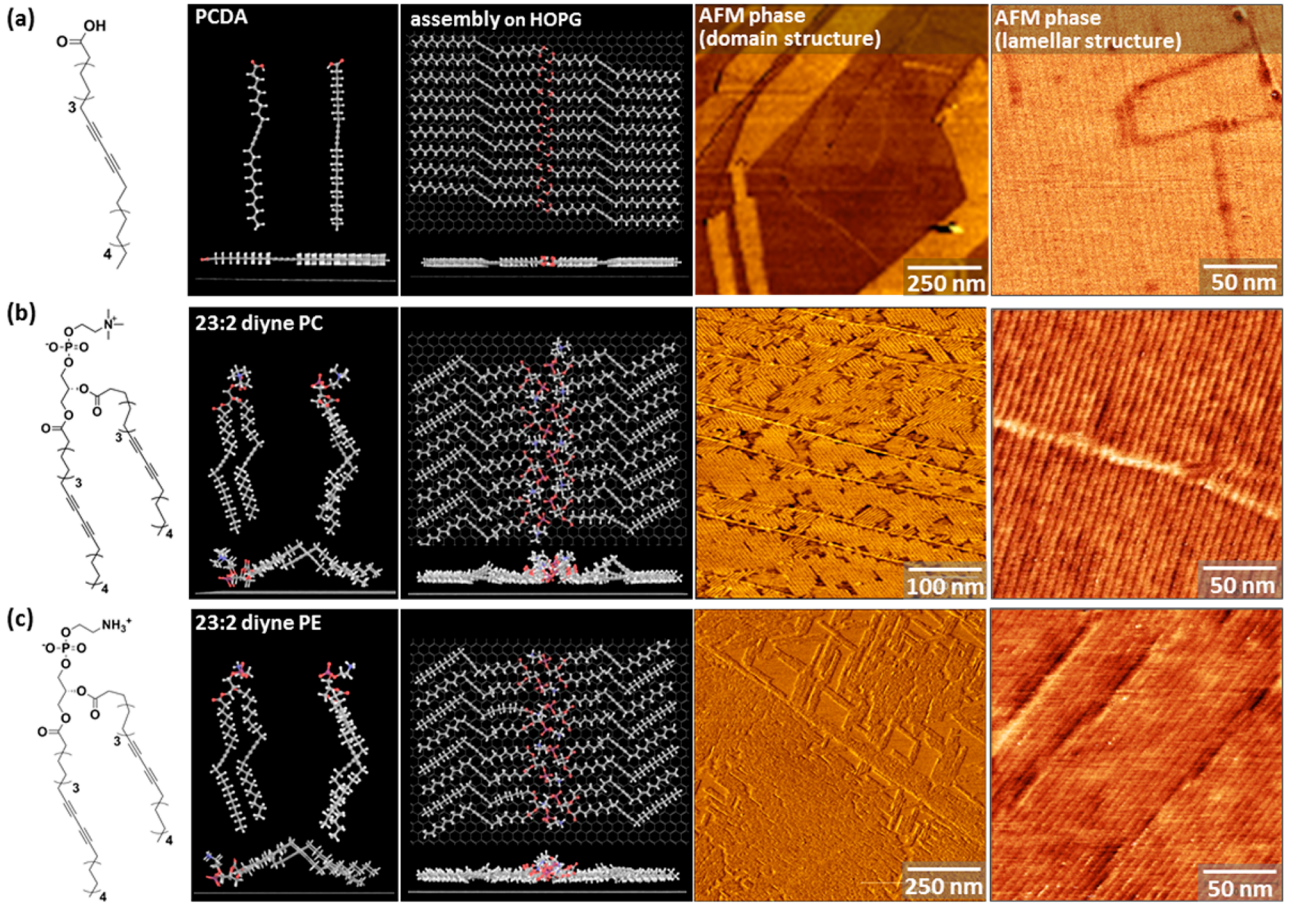

Figure 1. Modeled structures and AFM images of self-assembled polymerizable amphiphiles on HOPG. The first column shows (a) PCDA, (b) diyne PC, and (c) diyne PE. For each molecule, the second column shows two views of the solvent-minimized molecular structure (top) and a view of the solvent structure adsorbed to HOPG (bottom). The adsorbed structures were minimized to create the models in the third column, showing top and side views of each monolayer. In the fourth column, AFM phase images show large domains of molecules oriented epitaxially on HOPG; high-resolution images in the fifth column reveal lamellar periodicities (~6 nm) commensurate with the head-to-head models shown in the second column.

we performed energy minimizations to examine which adsorption geometry is preferred, an issue that would impact which functional groups in the head are most solvent-accessible.

AFM images of all three molecules deposited on HOPG reveal similar striped patterns with domains arranged at ~120° angles, characteristic of epitaxy with the hexagonal HOPG lattice, as expected from previous experiments with diynoic acids.[44] Line scans extracted from high-resolution AFM images exhibit lamellar periodicities of 6.3 ± 0.1 nm for diyne PE and 6.6 ± 0.1 nm for diyne PC. This is in good agreement with the modeled widths of double lamellae (6.0 nm for diyne PE and 6.4 nm for diyne PC) plus a van der Waals contact distance. Importantly, this suggests that the head-to-head structure is energetically preferred for both phospholipids, since a head-to-tail arrangement would likely produce features with ~3 nm periodicity.

Unlike the diynoic acids, both diyne phospholipids contain a chiral center in the headgroup, creating multiple possible adsorption geometries. Phospholipids may adsorb with the phosphate $(-PO_2-)^-$ facing the substrate, increasing the solvent accessibility of the amine (and presumably partly screening the phosphate charge), or they may adsorb with the phosphate proximal to the solvent and the amine adjacent to the surface. To test which configuration is more energetically favorable, we created models consisting of two adjacent rows of eight diyne lipids each adsorbed to a stack of two graphene sheets (see the Supporting Information), with all molecules adsorbed in either a phosphate-down configuration (Figure 2a) or a phosphate-up configuration (Figure 2b). Additionally, because the phosphocholine and phosphoethanolamine headgroups are narrower than the combined width of the two alkyl tails, it is possible to envision that headgroups from adjacent rows might interdigitate, leading to a configuration in which phosphates from one row lie next to the terminal amine or ammonium groups of molecules in the adjacent row. Such an interdigitated structure would be expected to increase the robustness of the monolayer, while likely decreasing the solvent accessibility of the headgroups. Therefore, we created sets of models in which molecules are initially positioned with interdigitated headgroups and models in which the rows are positioned 4 Å further apart, producing a noninterdigitated initial headgroup configuration. Minimization results in chloroform are presented in Figure 2c, as an energy difference between phosphate-down and phosphate-up adsorption geometries, expressed in units of eV/molecule (1 eV/molecule ≈ 96 kJ/mol). Both interdigitated and noninterdigitated initial headgroup configurations lead to an energetic preference of 0.6−0.7 eV/molecule for the phosphate-down configuration. Analyzing contributions from van der Waals and electrostatic interactions, strain, and solvation reveals that the preference

DOI: 10.1021/jacs.5b13179
J. Am. Chem. Soc. 2016, 138, 4448−4457

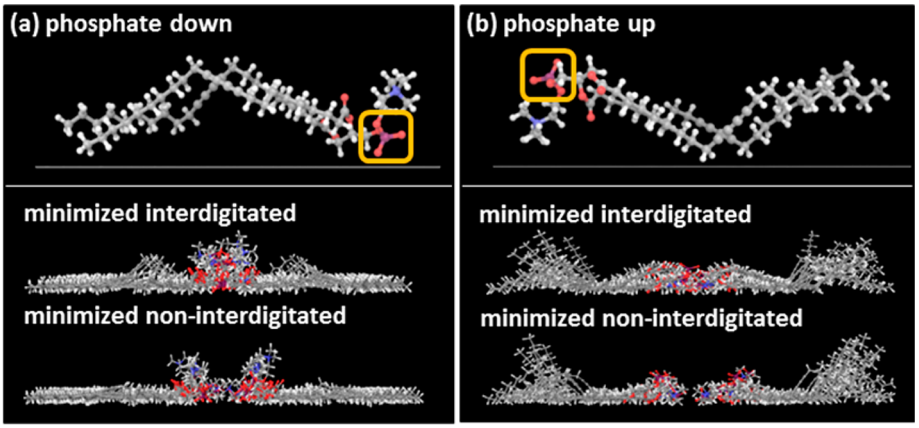

(c) $\Delta E = E_{\text{phosphate up}} - E_{\text{phosphate down}}$

	ΔE_{total} (eV/molecule)	ΔE_{vdW}	$\Delta E_{electrostatic}$	ΔE_{strain}	$\Delta E_{solvation}$
interdigitated	0.65	0.99	-0.12	-0.24	0.02
non-interdigitated	0.67	1.21	-0.35	-0.29	0.09

green indicates phosphate down adsorption energetically preferred; red/orange indicates phosphate up preferred

Figure 2. Minimizations of amphiphiles in phosphate-down and phosphate-up adsorption geometries. Minimized models of rows of molecules adsorbed in (a) phosphate-down and (b) phosphate-up configurations reveal greater tail group ordering for the phosphate-down configuration in both interdigitated and noninterdigitated headgroup configurations. (c) Energy differences between the two adsorption configurations indicate that the phosphate-down conformation is preferred due to increased van der Waals interactions.

arises from increased van der Waals interactions in the phosphate-down configuration. This is qualitatively visible in side views of the minimized models (Figure 2a,b) as increased ordering of the tail groups for phosphate-down structures in comparison with those of phosphate-up structures.

On the basis of modeling, it is not evident whether interdigitated headgroups would be preferred; however, a comparison of calculated and experimental lamellar widths suggests that the peripheries of the lamellar structures are not interdigitated. Minimizations of interdigitated structures lead to slightly smaller calculated average lamellar widths (5.8 nm for diyne PE and 5.7 nm for diyne PC) than those calculated for noninterdigitated structures (6.0 and 6.4 nm, vide supra). For diyne PC in particular (presumably due to the larger steric bulk of the terminal quaternary ammonium group), this leads to a relatively large difference between the modeled structure width and the structural periodicity observed experimentally in AFM images. Therefore, we postulate that the surface-adsorbed lipids adopt a noninterdigitated headgroup organization, which would increase the steric freedom of the terminal functional groups in comparison with an interdigitated structure.

Polymerization of Diyne Phospholipids. While individual molecules are relatively weakly adsorbed at the interface, surface-templated polymerization provides a route for increasing monolayer stability. Because diynoic acid monolayers on HOPG are known to undergo surface-templated photopolymerization,[40,44] it is reasonable to expect the same reactivity from the diynoic lipids we use here. However, a key structural consideration prompted us to examine molecular models to further explore the likelihood of polymerization: adjacent chains in lipid lamellae are bound together through the phospholipid headgroup, while the chains in diynoic acid lamellae are not.

Such a consideration is important in the context of this surface-templated reaction for two reasons. First, photopolymerization rates for diynes are known to depend strongly on the distance between the two bond-forming carbons in the crystal. In 3D crystals of smaller diynes (particularly *p*-toluenesulfonate hexadiyne),[57,58] increases of 1.0 Å between the bond-forming carbons correspond to a 2-fold decrease in polymerization rate. Similar constraints hold in 2D domains of diacetylene; in addition to decreasing polymerization efficiency with increasing separation between bond-forming carbons, studies of diynoic acids on HOPG and MoS_2 suggest differences in organization and polymerization behavior based on differences in lattice constants and work functions of the substrates.[42,46] For instance, on MoS_2, polymerization efficiency is ∼4 times higher than on HOPG, due to the increased conformational freedom afforded to alkyl chains in weaker epitaxy with the MoS_2 lattice.[46] A second structural consideration for polymerization is that the diyne functional group undergoes a rotation of ∼45° in the plane of the substrate in order to join the growing ene−yne polymer chain.[57] Therefore, it is possible that the additional constraints placed on chains joined through a headgroup would prevent them from undergoing polymerization.

With these considerations in mind, we compare the average distance (D_{10-13}) between bond-forming carbons (C10 of one chain and C13 of the adjacent chain) in monolayers of PCDA with those for the diyne phospholipid monolayers we form here. In calculating the C10−C13 distances for lipids, we examine pairs of chains both within a single molecule and between adjacent molecules. Minimized models of the diyne lipids show D_{10-13}(diyne PC) = 4.1 Å, comparable to D_{10-13}(PCDA) = 4.0 Å. In addition, the initial angle Θ between the diyne and the lamellar axis is slightly smaller for the phospholipids (Θ_{PCDA} = 59°, $\Theta_{\text{diyne PC}}$ = 51°), leading to

DOI: 10.1021/jacs.5b13179
J. Am. Chem. Soc. 2016, 138, 4448−4457

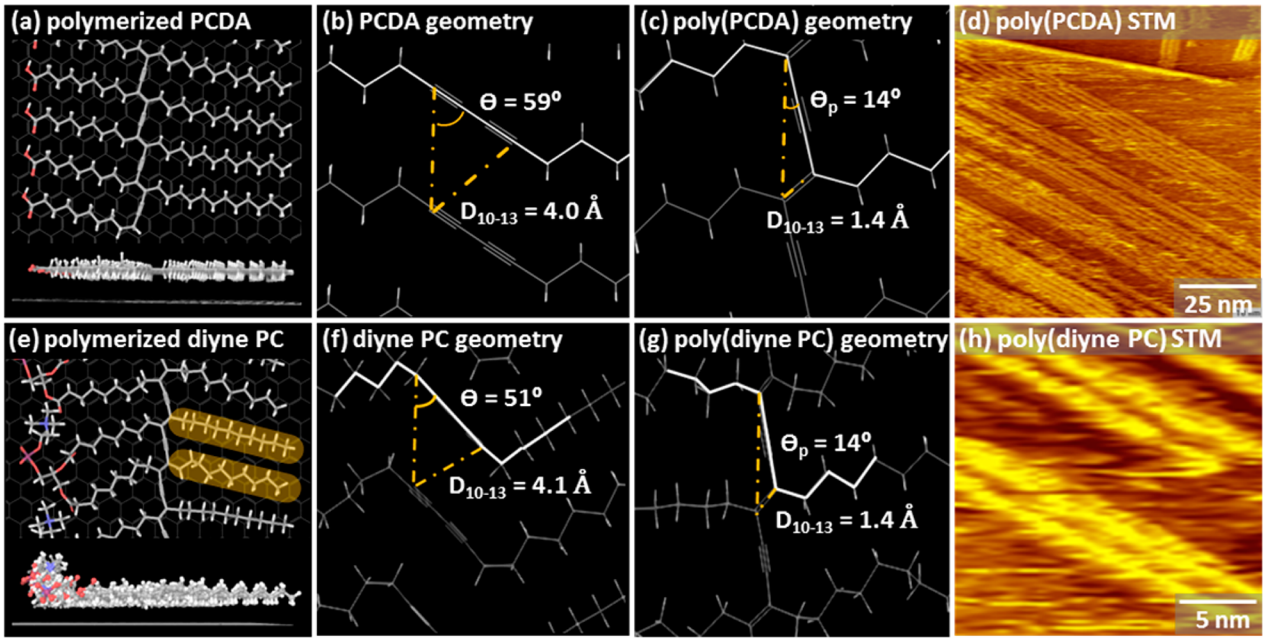

Figure 3. Energy-minimized molecular models and STM images showing polymerized (a–d) PCDA and (e–h) diyne PC. Minimized models of (b) unpolymerized PCDA and (f) diyne PC show that the distance between bond-forming carbons (D_{10-13}) and the angle between diyne and lamellar axis (Θ) are similar for the two molecules. STM images of polymerized (d) PCDA and (h) diyne PC show apparent protrusions corresponding to the conjugated ene–yne polymer. Highlighting in panel e indicates the alternating alkyl chain orientation probed in Figure 5.

favorable reduced rotational angles relative to PCDA ($\Delta\Theta_{PCDA}$ = 45°, $\Delta\Theta_{diyne\ PC}$ = 34°).

STM images of polymerized diynes are known to exhibit features with increased apparent height due to formation of the conjugated ene–yne polymer backbone.[4,40] Figure 3 shows STM images of polymerized diynoic acids (Figure 3d) and polymerized diyne PC (Figure 3h). Apparent protrusions in the image appear corresponding to modulations in both the topography and the local density of electronic states (LDOS). The relatively small HOMO–LUMO gap in polymerized diacetylenes vs diacetylene monomers increases the LDOS near the Fermi level, increasing the probability of electron tunneling;[41] although the native band gap of bulk polydiacetylenes is 2.3–2.5 eV, p-doping from HOPG substrates can reduce the band gap to as little as 0.5 eV.[42] Imaging at sufficiently large negative sample biases (here, V_s = −1.5 V) facilitates a two-step tunneling process that proceeds through the polydiacetylene wire.[41,59] While a number of studies provide experimental evidence suggesting that PCDA and other diynoic acids form a polymerized structure in which the ene–yne polymer is elevated ∼1.4 Å in relation to the surrounding alkyl chains,[40,44] DFT studies suggest that the lifted and in-plane polymer structures are similar in energy,[60] and in our simulations, models of both polymerized PCDA and diyne PC minimize to in-plane structures, though experimentally we find the standard linear features (Figure 3d) observed previously in STM images of polymerized PCDA. Previous studies imaging monolayers of long-chain diynes that do not form hydrogen-bonded dimers between headgroups (e.g.17,19-hexatriacontadiyne) find a transition from a lifted phase at 220 K to the in-plane conformation at room temperature,[61] which lacks the protruding linear features visible in STM images of PCDA. Here, while we observe the appearance of some linear features in STM images of polymerized diyne phospholipids (Figure 3h), the surface density of such features is lower than for PCDA, which could indicate either lower polymerization efficiency or the formation of an in-plane polymerized phase, as indicated in the minimized model (Figure 3e).

Because our primary interest is in the wetting properties of the interface, we use a washing assay to assess the impact of the polymerization on improving film robustness toward solvent. Samples of unpolymerized and polymerized amphiphiles were imaged and then subjected to sequential washing and imaging cycles to understand the extent to which washing removed molecules from the monolayer. Ethanol was used as a low surface tension washing solvent. Samples were washed vigorously with a stream of solvent from a squeeze bottle for 5-s intervals and then blown dry using compressed nitrogen gas. Figure 4 shows prewash and postwash images for unpolymerized and polymerized PCDA and diyne PE. Polymerized PCDA (Figure 4b) exhibits enhanced stability relative to unpolymerized PCDA (Figure 4a), demonstrating well-resolved lamellar structures within the domains throughout the washing procedure, although molecules at domain edges were eroded. The destabilizing effect of washing is also reflected in the increasing streakiness of the domain images, typically indicative of the presence of loose molecules. Conversely, a substantial fraction of the surface of the unpolymerized PCDA sample appeared bare after 5 s of washing, with only sparsely distributed aggregates of PCDA still visible, appearing as dark islands in the phase insets. In contrast, washing unpolymerized diyne PE (Figure 4c) resulted in slow etching of domain edges, with ∼40% of the surface containing ordered domains even after 30 s of washing. For polymerized diyne PE (Figure 4d), etching around domain edges was much slower, and ∼80% of the surface remained covered after 30 s of washing. We postulate that the enhanced stability of both polymerized and unpolymerized phospholipids relative to the diynoic acids may result from the increased number of alkyl carbons per molecule.

Molecular models suggest substantial differences in alkyl chain orientation between PCDA and the diyne phospholipids

DOI: 10.1021/jacs.5b13179
J. Am. Chem. Soc. 2016, 138, 4448–4457

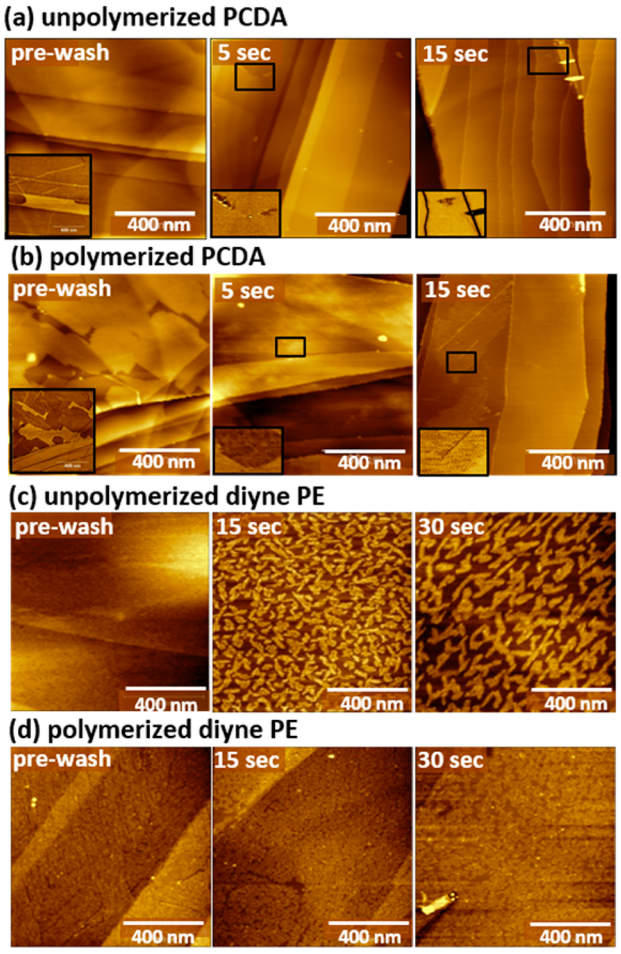

Figure 4. Solvent washing assay for unpolymerized and polymerized PCDA (a and b) and diyne PE (c and d) shows the enhanced stability of polymerized monolayers in comparison with unpolymerized monolayers and increased stability of diyne PE vs PCDA. Insets of panels a and b show phase images of the entire images or the corresponding scanned areas marked by the black square.

(Figure 3a,e). In PCDA, strong hydrogen-bonding interactions in carboxylic acid dimers order the headgroups, and tails form a tightly packed lattice with the zigzag backbone of the alkyl chains parallel to the HOPG surface.[40] In contrast, our models suggest that the lipid headgroups are somewhat disordered due to the three-dimensional geometry around the glycerol backbone. Our models also suggest that the lipid tail groups form an unusual structure in which the alkyl chains alternately zigzag parallel and perpendicular to the HOPG surface (highlighted in Figure 3e). Polarization modulated IR reflection absorption spectroscopy (PM-IRRAS)[62] measurements of films of PCDA and diyne lipids on HOPG exhibit substantial differences in C−H stretch intensity (Figure 5a) consistent with this difference in ordering. Ester C═O stretch peak intensities for diyne PC are also reduced relative to PCDA C═O stretch intensities (Figure 5b), consistent with energy-minimized models, suggesting that the ester linkage adopts a variety of configurations relative to the surface normal, in order to bring the two diynes into alignment as the lipid conforms to the graphite surface.

Controlling the Charge State of Surface Functional Group Patterns. The difference in placement of the phosphate and amine functional groups relative to the interface

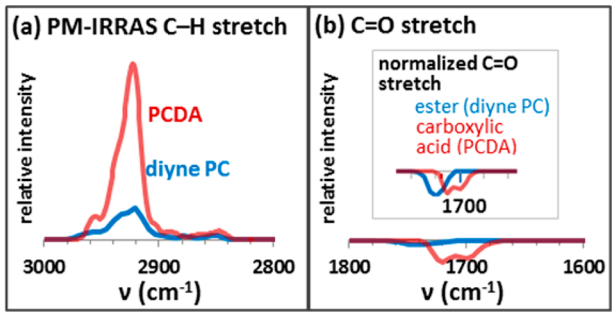

Figure 5. PM-IRRAS spectra of films of PCDA and diyne PC exhibit differences in (a) C−H and (b) C═O stretch intensities consistent with alkyl chain orientation differences observed in energy-minimized molecular models.

is expected to impact their ionization and, thus, interactions with solvents and analytes.

A number of techniques, including differential capacitance measurements,[63] nonlinear optical spectroscopy,[64] and contact angle goniometry,[48] can be used to assess ionization behavior at interfaces. Here, we use contact angle titration, in which a series of small droplets of buffers with controlled pH are applied to the interface; the contact angles of the buffer droplets change in pH ranges corresponding to the ionization of functional groups at the interface.[48] Interfacial $pK_{1/2}$ values are known to differ substantially from pK_as of the same functionalities in solution. For instance, the pK_a of acetic acid in dilute aqueous solution is ∼4.7.[65] However, previously it has been shown that both carboxylic acid-terminated SAMs and oxidized polymer films displaying carboxylic acids typically exhibit $pK_{1/2}$ values of 7−8.[48] Similarly, $pK_{1/2}$ values of amines in alkanethiol SAMs typically *decrease* relative to pK_a values in aqueous solutions. While the pK_a of dilute methylamine in aqueous solution is 10.5,[49] one study measured a $pK_{1/2}$ of 6.5 for an NH_2-terminated undecanethiol SAM, lower than the measured $pK_{1/2}$ of 7.4 for a COOH-terminated undecanethiol SAM measured in the same work.[49] Both shifts can be understood by considering the equilibrium between charged and neutral forms of the molecules; in both amines and carboxylic acids, proximity to the nonpolar interface decreases stabilization of the charged form of the functional group, shifting the equilibrium toward the neutral form. Similarly, $pK_{1/2}$ has been shown to vary with the surface density of functional groups in a SAM.[48] For a 75% COOH-terminated alkyl SAM, the measured $pK_{1/2}$ was 8.5, while for a lower-coverage 15% COOH-terminated alkyl SAM, the $pK_{1/2}$ shifted as high as 11.

Both surface shifts and those due to fractional coverage are important in predicting the ionization behavior of functional groups in the monolayers prepared here. Figure 1a shows that for PCDA monolayers, approximately 10% of the surface consists of ionizable functional groups. However, the chemical environment of the carboxylic acid groups is more similar to that which would be found in a high-percentage COOH-terminated alkyl thiol SAM, since the functionalities are clustered at the lamellar edges.

Figure 6 shows the results of contact angle titrations for pentacosane, PCDA, diyne PC, and diyne PE. For films of pentacosane (Figure 6a), a 25-carbon alkane, on HOPG, contact angles are ∼98° across the tested pH range (1−13). For PCDA (Figure 6b, squares = advancing, circles = receding), contact angles are lower than for pentacosane due to the introduction of the polar carboxylic acid functional group.

DOI: 10.1021/jacs.5b13179
J. Am. Chem. Soc. 2016, 138, 4448−4457

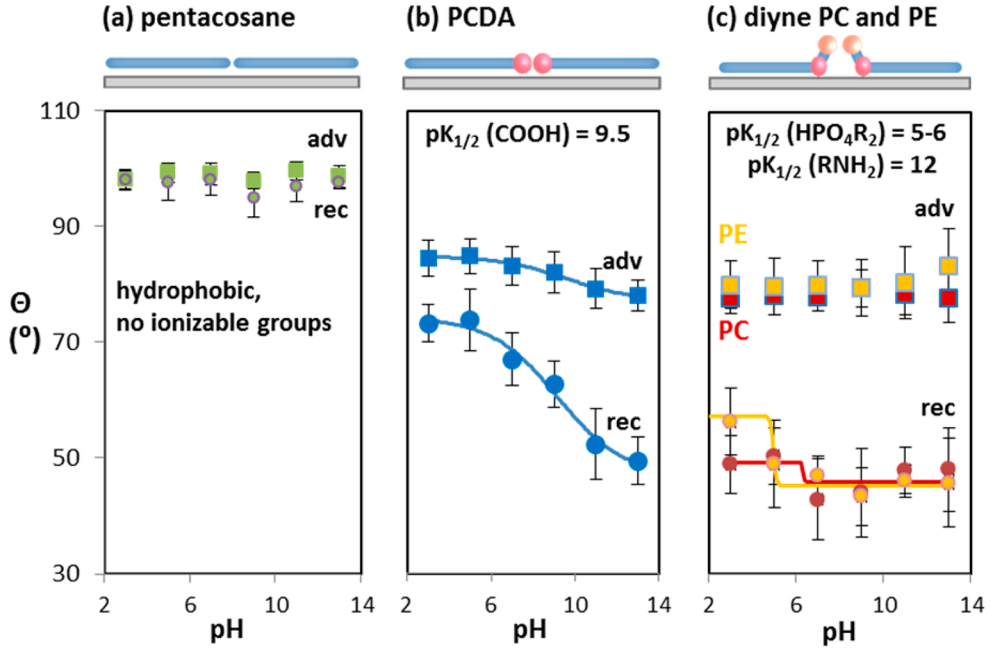

Figure 6. Contact angle titrations showing changes in contact angle with buffer pH for HOPG with adsorbed (a) pentacosane, (b) polymerized PCDA, and (c) polymerized diyne lipids PC and PE. Square markers indicate advancing contact angles; circles indicate receding contact angles. Error bars indicate the standard deviation in angle over a series of nine measurements acquired from three different samples.

Below pH 5, the carboxylic acids are neutral, leading to advancing contact angles of ~84°. We correlate this decrease with the fractional surface coverage of carboxylic acids using a modified form of the Young–Dupré equation for interfaces with nanoscale chemical heterogeneity:[66]

$$(1 + \cos\theta_{PCDA})^2 = f_{alkyl}(1 + \cos\theta_{alkyl})^2 + f_{COOH}(1 + \cos\theta_{COOH})^2$$

Using the measured contact angle of 98° for alkyl chains aligned epitaxially on HOPG, 84° for neutral PCDA, and 30° for neutral COOH groups (value observed in previous contact angle measurements on 100% COOH-terminated alkyl thiol SAMs[48]), the observed decrease in contact angle relative to pentacosane would be expected for an 18% surface coverage of neutral carboxylic acid groups, consistent with moderate disordering of the COOH groups during wetting. We note that it is not entirely clear that the contact angle for a lying-down phase of COOH dimers would be exactly the same as that (30°) for a standing phase of alkanethiol-terminated COOH groups and that, if the bond dipoles in the carboxylic acid are oriented in the plane of the monolayer, this would lead to a somewhat higher water contact angle. Using a larger contact angle in the above equation results in a higher calculated f_{COOH}, implying more disordering at the interface and a disruption of the COOH dimers along the periphery of the lamellar structure. This reorientation would produce hydrophilic areas with unpaired –COOH groups more closely resembling standing-phase COOH-terminated alkanethiols. Thus, the calculated hydrophilic surface coverage of 18% should be considered an approximate but reasonable minimum.

With increasing pH, the carboxylic acids begin to ionize, further decreasing both advancing and receding angles. On the basis of the receding angles (blue circles), in which the larger change in contact angle makes the transition more evident, we estimate an onset of ionization at pH 5 and a $pK_{1/2}$ of 9.5, using a sigmoidal fit (blue line). Therefore, while the $pK_{1/2}$ is shifted due to the nonpolar environment at the interface, clustering the carboxylic acid groups at lamellar edges decreases the $pK_{1/2}$ relative to the value of 11 measured previously for 15% COOH-terminated standing phases of alkanethiol SAMs on Au(111).[48]

In contrast with PCDA, diyne PC (Figure 6c, red squares = advancing; red circles = receding) has a terminal quaternary ammonium group that remains charged across the pH range, leading to advancing contact angles ~74°, similar to those for the ionized form of PCDA. Although the ammonium group remains charged, at low pH, the phosphate group can become protonated. While the solution pK_a for a phosphocholine phosphate is 1, here we observe a $pK_{1/2}$ of approximately 5.9, consistent with the interfacial pK_a shift of the carboxylic acid in PCDA. Similarly, for diyne PE, an increase in receding contact angle is observed at low pH (Figure 6c, yellow circles), with a calculated $pK_{1/2}$ = 4.9. This sigmoidal fit was calculated using additional data points below pH 3 to improve accuracy (see the Supporting Information).

The diyne PE primary amine has a solution pK_a of 11. A small increase in the advancing contact angle is observed near pH 11 (Figure 6c, yellow squares), consistent with neutralization of the amine. No corresponding increase in receding angle is observed (Figure 6c, yellow circles), presumably because the phosphate group remains charged and can influence the receding angle more strongly than the advancing angle. Importantly, this suggests that the diyne PE amine does not undergo a significant interfacial $pK_{1/2}$ shift due to its separation from the hydrophobic interface and the proximity of the charged phosphate group.

■ CONCLUSIONS AND PROSPECTS

Here, we have demonstrated a route for functionalization of layered materials based on sitting phases of polymerizable lipids. The lipids contain multiple functional groups (phosphate and amine or ammonium) that are precisely positioned relative

DOI: 10.1021/jacs.5b13179
J. Am. Chem. Soc. 2016, 138, 4448–4457

to the layered material interface. Because the phosphate sits close to the interface, it experiences a pK_a shift characteristic of functional groups at hydrophobic interfaces; conversely, the terminal primary amine in diyne PE, which projects just a few angstroms above the interface, maintains its standard solution ionization behavior. This difference points to the ability to tailor chemical characteristics of the interface by varying the functionalities present in the lipid headgroup and their positions relative to the interface.

On the basis of the diversity of natural lipids (over 100 unique lipids have been identified to date),[50] it is reasonable to suppose that a large amount of structural and chemical diversity can be introduced into monolayers using this strategy. In biology, lipids are known to play roles in stabilizing membrane curvature and junctions, protein interactions, regulating cell growth, and biosynthetic pathways, suggesting the possibility that similarly diverse functions could be stably integrated with layered materials.

EXPERIMENTAL METHODS

Amphiphile Monolayer Preparation. Diacetylene-functionalized phospholipids and fatty acids were purchased from suppliers indicated and used as received: 1,2-bis(10,12-tricosadiynoyl)-*sn*-glycero-3-phosphocholine (Avanti Lipids, Alabaster, AL, >99.0% purity), 1,2-bis(10,12-tricosadiynoyl)-*sn*-glycero-3-phosphoethanolamine (Avanti, >99.0% purity), 10,12-pentacosadiynoic acid (Sigma-Aldrich, St. Louis, MO, ≥97.0% purity), and 10,12-nonacosadiynoic acid (Tokyo Chemical International, Tokyo, Japan, >97.0% purity). Chloroform, hexane, and isopropyl alcohol (ChromAR grade) were purchased from Macron Fine Chemicals (Center Valley, PA) and used as received. Self-assembled monolayers of diacetylene-functionalized lipids and fatty acids were prepared either by drop-casting or Langmuir−Schaefer (LS) deposition as described below. In both techniques, polymerizable amphiphiles were deposited on 1 × 1 cm highly oriented pyrolytic graphite (HOPG, SPI Supplies, West Chester, PA) substrates, which were freshly cleaved immediately prior to sample deposition. All initial steps in the deposition process were carried out under UV-filtered light to prevent polymerization in solution.

For samples prepared by drop-casting, monolayers of lipids and fatty acids were formed by placing 6 μL of a 0.015−0.017 mg/mL solution of the functional molecule in a 3:2 (v/v) mixture of hexane:isopropyl alcohol on a heated (90−107 °C) HOPG substrate. LS deposition was performed using a KSV-NIMA Langmuir−Blodgett trough (Biolin Scientific, Stockholm, Sweden). For the deposition of fatty acids, 12 μL of a 0.75 mg/mL solution of fatty acid in chloroform was deposited on a subphase of deionized water (~18 MΩ). For phospholipid monolayers, deposition was performed by spreading 15−20 μL of a 0.5 mg/mL solution of lipid in chloroform onto a subphase of aqueous 5 mM $MnCl_2$. After the small amount of chloroform used for amphiphile transfer was allowed to evaporate, trough barriers were slowly moved inward to adjust the surface pressure. When the surface pressure reached 10 mN/m, the HOPG substrate was slowly lowered onto the subphase with the cleaved surface facing down, parallel to the liquid interface. After 4 min in contact with the liquid interface, the HOPG was gently lifted out of contact with the liquid using the automatic dipper.

Diacetylene-functionalized amphiphile monolayers prepared using the described procedure were photopolymerized by 1 h of irradiation under a 254-nm 8-W UV lamp with approximately 4 cm between the lamp and the sample surface.

AFM Imaging. All AFM measurements were performed under ambient conditions using a Veeco MultiMode (Bruker Instruments, Billerica, MA) instrument in tapping mode with Nanoprobe (Neuchatel, Switzerland) PPP-FM or RFESP-75 tips (nominal force constant 3 N/m and radius of curvature <10 nm).

STM Imaging. STM images were acquired using a custom-built ambient STM[67−69] with a Besocke-type head design and RHK-R9 control electronics (RHK Technology, Troy, MI). STM tips were prepared mechanically from Pt/Ir alloy wire (Goodfellow, Pt 90%, Ir 10%). Imaging was performed in constant current mode with a tip bias of 1.5 V and tunneling current set point of 7 pA.

Energy Minimization. Software packages Maestro[46] and Macromodel[47] (Schrödinger, Cambridge, MA) were used, respectively, to visualize the structures of phospholipids and fatty acids on graphene and to perform the force field minimizations and molecular dynamics simulations. All models were minimized using the OPLS_2005 force field,[48] with normal cutoffs for van der Waals, electrostatic, and hydrogen-bonding interactions. Minimizations were performed using the Polak−Ribiere conjugate gradient (PRCG) algorithm and gradient method with 50 000 runs and a convergence threshold of 0.05. Most minimizations converged in less than 10 000 runs. For all calculations, atoms in the graphene sheets were frozen, to more closely mimic the structure of HOPG. Thus, while they contributed to the forces present in the system, their positions did not change in response to conformational changes of the adsorbed amphiphiles. For simulations using aqueous buffers, molecular dynamics simulations were carried out using explicit water and ions to simulate 5 mM $MnCl_2$ (see the Supporting Information). Briefly, 1680 water molecules, 19 Mn^{2+} ions, and 38 Cl^- were positioned with appropriate spacings over graphene sheets identical to those used in chloroform and solvent-free minimizations. Molecular dynamics simulations were run for 200 ps; models were subsequently reminimized and energy values tabulated as for other models.

Contact Angle Titrations. Contact angle titrations were performed using an Attension Theta optical tensiometer (Biolin Scientific, Stockholm, Sweden) in sessile drop mode. Buffers with 20 mM buffering capacity at a range of pH values from 1 to 14 were purchased from Sigma-Aldrich and used as received. The pH of each buffer was measured prior to utilization in contact angle measurements to ensure that the measured pH was within 0.2 units of the stated pH. For each measurement, a 5-μL droplet of buffer solution at the stated pH was deposited on a prepared sample of polymerized amphiphile on HOPG, and the contact angle was measured within 10 s and recorded as the advancing contact angle. Subsequently, solvent was withdrawn from the droplet using a syringe with a 32-gauge needle, until the solvent front on the sample receded. The contact angle was measured at this point and recorded as the receding contact angle. Each contact angle graphed in the paper represents the average of nine points (three points measured on each of three different samples). Typically, it was possible to acquire a grid of nine measurements per 1 × 1 cm sample.

PM-IRRAS. Spectra were acquired using a custom-built PM-IRRAS spectrophotometer. The infrared light source, interferometer, and data collection and processing were provided by a Nicolet iS50R spectrometer (Thermo, Waltham, MA). All optical components were purchased from Thorlabs (Newton, NJ) unless otherwise specified. The infrared beam was passed from the spectrometer exit port into a polycarbonate enclosure and directed through a KRS-5 lens at a 70° incidence angle using AR coated gold mirrors. The beam then passed through a holographic BaF_2 linear polarizer set at an angle of 45° relative to the optical axis of a Hinds Series II ZNS50 photoelastic modulator (Hinds Instruments, Portland, OR), which modulated the beam at a 50 kHz frequency with the half-wave retardation set to 2100 cm^{-1}. The beam was then focused onto the sample and reflected through a second BaF_2 linear polarizer, which was adjusted to minimize the polarization effects of the substrate. Finally, the light was focused through a BaF_2 lens onto a HgCdTe high D* detector (Thermo, Waltham, MA). Spectra were acquired at 8 cm^{-1} resolution and normalized by dividing a spectrum of the substrate with a monolayer by a spectrum of a bare substrate.

ASSOCIATED CONTENT

Supporting Information

The Supporting Information is available free of charge on the ACS Publications website at DOI: 10.1021/jacs.5b13179.

DOI: 10.1021/jacs.5b13179
J. Am. Chem. Soc. 2016, 138, 4448−4457

Additional descriptions of molecular models, contact angle repeatability profiling, and data used for sigmoidal curve fitting of diyne PE below pH 3 (PDF)

AUTHOR INFORMATION

Corresponding Author

*claridge@purdue.edu

Author Contributions

J.J.B. and K.K.R. contributed equally to this work.

Notes

The authors declare no competing financial interests.

ACKNOWLEDGMENTS

S.A.C. and J.J.B. acknowledge support through an ACS Petroleum Research Fund Doctoral New Investigator Award (PRF# 54763-DNI5), and S.A.C. acknowledges support through an NSF CAREER award (NSF-CHE 1555173). S.R.R. has been supported through a W. Brooks Fortune Predoctoral Fellowship and a Frederick N. Andrews Predoctoral Fellowship. The authors are grateful to D. Thompson for helpful discussions, and D. McMillan and H. Hedderich for technical assistance.

REFERENCES

(1) Groves, J. T.; Ulman, N.; Boxer, S. G. *Science* **1997**, *275*, 651.
(2) Cremer, P. S.; Boxer, S. G. *J. Phys. Chem. B* **1999**, *103*, 2554.
(3) Groves, J. T.; Boxer, S. G. *Acc. Chem. Res.* **2002**, *35*, 149.
(4) Claridge, S. A.; Liao, W.-S.; Thomas, J. C.; Zhao, Y.; Cao, H. H.; Cheunkar, S.; Serino, A. C.; Andrews, A. M.; Weiss, P. S. *Chem. Soc. Rev.* **2013**, *42*, 2725.
(5) Bain, C. D.; Troughton, E. B.; Tao, Y. T.; Evall, J.; Whitesides, G. M.; Nuzzo, R. G. *J. Am. Chem. Soc.* **1989**, *111*, 321.
(6) Nuzzo, R. G.; Dubois, L. H.; Allara, D. L. *J. Am. Chem. Soc.* **1990**, *112*, 558.
(7) Laibinis, P. E.; Whitesides, G. M.; Allara, D. L.; Tao, Y. T.; Parikh, A. N.; Nuzzo, R. G. *J. Am. Chem. Soc.* **1991**, *113*, 7152.
(8) Love, J. C.; Estroff, L. A.; Kriebel, J. K.; Nuzzo, R. G.; Whitesides, G. M. *Chem. Rev.* **2005**, *105*, 1103.
(9) Poirier, G. E. *Chem. Rev.* **1997**, *97*, 1117.
(10) Burda, C.; Chen, X. B.; Narayanan, R.; El-Sayed, M. A. *Chem. Rev.* **2005**, *105*, 1025.
(11) Alivisatos, A. P. *Science* **1996**, *271*, 933.
(12) Steigerwald, M. L.; Brus, L. E. *Acc. Chem. Res.* **1990**, *23*, 183.
(13) Murray, C. B.; Kagan, C. R.; Bawendi, M. G. *Annu. Rev. Mater. Sci.* **2000**, *30*, 545.
(14) Shirasaki, Y.; Supran, G. J.; Bawendi, M. G.; Bulovic, V. *Nat. Photonics* **2013**, *7*, 13.
(15) Claridge, S. A.; Castleman, A. W.; Khanna, S. N.; Murray, C. B.; Sen, A.; Weiss, P. S. *ACS Nano* **2009**, *3*, 244.
(16) Alivisatos, A. P.; Gu, W. W.; Larabell, C. *Annu. Rev. Biomed. Eng.* **2005**, *7*, 55.
(17) Alivisatos, A. P.; Johnsson, K. P.; Peng, X. G.; Wilson, T. E.; Loweth, C. J.; Bruchez, M. P.; Schultz, P. G. *Nature* **1996**, *382*, 609.
(18) Manna, L.; Scher, E. C.; Alivisatos, A. P. *J. Am. Chem. Soc.* **2000**, *122*, 12700.
(19) Mirkin, C. A.; Letsinger, R. L.; Mucic, R. C.; Storhoff, J. J. *Nature* **1996**, *382*, 607.
(20) Park, S. Y.; Lytton-Jean, A. K. R.; Lee, B.; Weigand, S.; Schatz, G. C.; Mirkin, C. A. *Nature* **2008**, *451*, 553.
(21) Butler, S. Z.; Hollen, S. M.; Cao, L.; Cui, Y.; Gupta, J. A.; Gutierrez, H. R.; Heinz, T. F.; Hong, S. S.; Huang, J.; Ismach, A. F.; Johnston-Halperin, E.; Kuno, M.; Plashnitsa, V. V.; Robinson, R. D.; Ruoff, R. S.; Salahuddin, S.; Shan, J.; Shi, L.; Spencer, M. G.; Terrones, M.; Windl, W.; Goldberger, J. E. *ACS Nano* **2013**, *7*, 2898.
(22) Geim, A. K. *Science* **2009**, *324*, 1530.
(23) MacLeod, J. M.; Rosei, F. *Small* **2014**, *10*, 1038.
(24) Mann, J. A.; Dichtel, W. R. *J. Phys. Chem. Lett.* **2013**, *4*, 2649.
(25) Kozbial, A.; Li, Z.; Conaway, C.; McGinley, R.; Dhingra, S.; Vahdat, V.; Zhou, F.; D'Urso, B.; Liu, H.; Li, L. *Langmuir* **2014**, *30*, 8598.
(26) De Feyter, S.; De Schryver, F. C. *Chem. Soc. Rev.* **2003**, *32*, 139.
(27) Giancarlo, L. C.; Flynn, G. W. *Acc. Chem. Res.* **2000**, *33*, 491.
(28) Cyr, D. M.; Venkataraman, B.; Flynn, G. W. *Chem. Mater.* **1996**, *8*, 1600.
(29) Giancarlo, L. C.; Flynn, G. W. *Annu. Rev. Phys. Chem.* **1998**, *49*, 297.
(30) Wei, Y. H.; Kannappan, K.; Flynn, G. W.; Zimmt, M. B. *J. Am. Chem. Soc.* **2004**, *126*, 5318.
(31) Elemans, J. A. A. W.; Lei, S.; De Feyter, S. *Angew. Chem., Int. Ed.* **2009**, *48*, 7298.
(32) Claridge, S. A.; Thomas, J. C.; Silverman, M. A.; Schwartz, J. J.; Yang, Y.; Wang, C.; Weiss, P. S. *J. Am. Chem. Soc.* **2013**, *135*, 18528.
(33) Mao, X.; Guo, Y.; Luo, Y.; Niu, L.; Liu, L.; Ma, X.; Wang, H.; Yang, Y.; Wei, G.; Wang, C. *J. Am. Chem. Soc.* **2013**, *135*, 2181.
(34) Furukawa, H.; Cordova, K. E.; O'Keeffe, M.; Yaghi, O. M. *Science* **2013**, *341*, 974.
(35) Samori, P.; Fechtenkotter, A.; Jackel, F.; Bohme, T.; Mullen, K.; Rabe, J. P. *J. Am. Chem. Soc.* **2001**, *123*, 11462.
(36) Gellman, A. J.; Paserba, K. R. *J. Phys. Chem. B* **2002**, *106*, 13231.
(37) Grim, P. C. M.; De Feyter, S.; Gesquiere, A.; Vanoppen, P.; Ruker, M.; Valiyaveettil, S.; Moessner, G.; Mullen, K.; De Schryver, F. C. *Angew. Chem., Int. Ed. Engl.* **1997**, *36*, 2601.
(38) Colson, J. W.; Woll, A. R.; Mukherjee, A.; Levendorf, M. P.; Spitler, E. L.; Shields, V. B.; Spencer, M. G.; Park, J.; Dichtel, W. R. *Science* **2011**, *332*, 228.
(39) Cui, D.; MacLeod, J. M.; Ebrahimi, M.; Perepichka, D. F.; Rosei, F. *Chem. Commun.* **2015**, *51*, 16510.
(40) Okawa, Y.; Aono, M. *J. Chem. Phys.* **2001**, *115*, 2317.
(41) Akai-Kasaya, M.; Shimizu, K.; Watanabe, Y.; Saito, A.; Aono, M.; Kuwahara, Y. *Phys. Rev. Lett.* **2003**, *91*, 255501.
(42) Giridharagopal, R.; Kelly, K. F. *ACS Nano* **2008**, *2*, 1571.
(43) Okawa, Y.; Aono, M. *Nature* **2001**, *409*, 683.
(44) Okawa, Y.; Akai-Kasaya, M.; Kuwahara, Y.; Mandal, S. K.; Aono, M. *Nanoscale* **2012**, *4*, 3013.
(45) Deshpande, A.; Sham, C.-H.; Alaboson, J. M. P.; Mullin, J. M.; Schatz, G. C.; Hersam, M. C. *J. Am. Chem. Soc.* **2012**, *134*, 16759.
(46) Mandal, S. K.; Okawa, Y.; Hasegawa, T.; Aono, M. *ACS Nano* **2011**, *5*, 2779.
(47) Tahara, K.; Katayama, K.; Blunt, M. O.; Iritani, K.; De Feyter, S.; Tobe, Y. *ACS Nano* **2014**, *8*, 8683.
(48) Bain, C. D.; Whitesides, G. M. *Langmuir* **1989**, *5*, 1370.
(49) Fears, K. P.; Creager, S. E.; Latour, R. A. *Langmuir* **2008**, *24*, 837.
(50) *Biochemistry of Lipids, Lipoproteins and Membranes*, 5th ed.; Vance, D. E., Vance, J. E., Eds.; Elsevier: New York, 2008.
(51) Marsh, D. *Handbook of Lipid Bilayers*, 2nd ed.; CRC Press: Boca Raton, FL, 2013.
(52) Shuster, M. J.; Vaish, A.; Szapacs, M. E.; Anderson, M. E.; Weiss, P. S.; Andrews, A. M. *Adv. Mater.* **2008**, *20*, 164.
(53) Vaish, A.; Shuster, M. J.; Cheunkar, S.; Singh, Y. S.; Weiss, P. S.; Andrews, A. M. *ACS Chem. Neurosci.* **2010**, *1*, 495.
(54) O'Brien, D. F.; Whitesides, T. H.; Klingbiel, R. T. *J. Polym. Sci., Polym. Lett. Ed.* **1981**, *19*, 95.
(55) Zhang, H.; Joubert, J. R.; Saavedra, S. S. *Adv. Polym. Sci.* **2009**, *224*, 1.
(56) Lopez, E.; O'Brien, D. F.; Whitesides, T. H. *J. Am. Chem. Soc.* **1982**, *104*, 305.
(57) Baughman, R. H. *J. Appl. Phys.* **1972**, *43*, 4362.
(58) Wegner, G. *Makromol. Chem.* **1971**, *145*, 85.
(59) Giridharagopal, R.; Kelly, K. F. *J. Phys. Chem. C* **2007**, *111*, 6161.
(60) Okawa, Y.; Takajo, D.; Tsukamoto, S.; Hasegawa, T.; Aono, M. *Soft Matter* **2008**, *4*, 1041.
(61) Endo, O.; Toda, N.; Ozaki, H.; Mazaki, Y. *Surf. Sci.* **2003**, *545*, 41.

DOI: 10.1021/jacs.5b13179
J. Am. Chem. Soc. 2016, 138, 4448−4457

(62) Russell, S. R.; Claridge, S. A. *Anal. Bioanal. Chem.* **2016**, DOI: 10.1007/s00216-015-9262-5.
(63) Bryant, M. A.; Crooks, R. M. *Langmuir* **1993**, *9*, 385.
(64) Zhao, X. L.; Subrahmanyan, S.; Eisenthal, K. B. *Chem. Phys. Lett.* **1990**, *171*, 558.
(65) *CRC Handbook of Chemistry and Physics*; 95th ed.; CRC Press, Inc.: Boca Raton, FL, 2014.
(66) Israelachvili, J. N. *Intermolecular and Surface Forces*, 3rd ed.; Elsevier: Waltham, MA, 2011.
(67) Bumm, L. A.; Weiss, P. S. *Rev. Sci. Instrum.* **1995**, *66*, 4140.
(68) Moore, A. M.; Yeganeh, S.; Yao, Y. X.; Claridge, S. A.; Tour, J. M.; Ratner, M. A.; Weiss, P. S. *ACS Nano* **2010**, *4*, 7630.
(69) Bang, J. J.; Russell, S. R.; Rupp, K. K.; Claridge, S. A. *Anal. Methods* **2015**, *7*, 7106.

DOI: 10.1021/jacs.5b13179
J. Am. Chem. Soc. 2016, 138, 4448−4457